ADVANCED MATERIALS

www.advmat.de

A Black Phosphorus Carbide Infrared Phototransistor

*Wee Chong Tan, Li Huang, Rui Jie Ng, Lin Wang, Dihan Md. Nuruddin Hasan, Thorin Jake Duffin, Karuppannan Senthil Kumar, Christian A. Nijhuis, Chengkuo Lee, and Kah-Wee Ang**

Photodetectors with broadband detection capability are desirable for sensing applications in the coming age of the internet-of-things. Although 2D layered materials (2DMs) have been actively pursued due to their unique optical properties, by far only graphene and black arsenic phosphorus have the wide absorption spectrum that covers most molecular vibrational fingerprints. However, their reported responsivity and response time are falling short of the requirements needed for enabling simultaneous weak-signal and high-speed detections. Here, a novel 2DM, black phosphorous carbide (b-PC) with a wide absorption spectrum up to 8000 nm is synthesized and a b-PC phototransistor with a tunable responsivity and response time at an excitation wavelength of 2004 nm is demonstrated. The b-PC phototransistor achieves a peak responsivity of 2163 A W^{-1} and a shot noise equivalent power of 1.3 fW Hz$^{-1/2}$ at 2004 nm. In addition, it is shown that a response time of 0.7 ns is tunable by the gating effect, which renders it versatile for high-speed applications. Under the same signal strength (i.e., excitation power), its performance in responsivity and detectivity in room temperature condition is currently ahead of recent top-performing photodetectors based on 2DMs that operate with a small bias voltage of 0.2 V.

Photodetectors are a key component of many devices we use in our daily life. From metrology and imaging to optical communications, we rely on photodetectors to convert the information stored in light into electrical signals that can be processed by standard electronics. Today, different technologically important wavelength regimes are detected by separate photoactive semiconductors with appropriate bandgaps. For example, gallium nitride, silicon (Si), and indium gallium arsenide (InGaAs) are typically exploited for sensing in the ultraviolet, visible, and near-infrared regimes while the detection of mid-infrared (MIR) wavelength generally relies on small-bandgap semiconductor compounds such as mercury cadmium telluride, lead sulfide (PbS) or lead selenide. Thermal sensing techniques are utilized for detection in the far-infrared (FIR) regime. However, the rapid proliferation of connectivity, availability of cloud computing, and miniaturization of sensors and communications chips have made it possible for many devices to be networked together to create the internet-of-things (IoT). Although the number of deployments is still relatively small, the demand is set to rise and organizations worldwide are pushing ahead for a broadband optical sensor that can covers as many important wavelength regimes as possible so that only one type of optical sensor is needed for the implementation of IoT. Recent years have witnessed many breakthroughs in the research on 2D layered materials (2DMs). Materials such as graphene,[1,2] semiconducting di- and trichalcogenides,[3–5] II–VI compound gallium telluride (GaTe),[6] black phosphorus (b-P),[7–10] and black arsenic phosphorus (b-AsP)[11] are all examples of 2DMs that may have an impact in high speed flexible optoelectronics in the coming years.[12] While photodetectors based on 2D materials (2DMs)[13] have atomic thickness and are more flexible than bulk semiconductor, by far only graphene[14] and b-AsP[11] have the wide

Dr. W. C. Tan, L. Huang, R. J. Ng, Dr. L. Wang, D. Md. N. Hasan, Prof. C. Lee, Prof. K.-W. Ang
Department of Electrical and Computer Engineering
National University of Singapore
4 Engineering Drive 3, Singapore 117583, Singapore
E-mail: eleakw@nus.edu.sg

Dr. W. C. Tan, L. Huang, R. J. Ng, Dr. L. Wang, Prof. K.-W. Ang
Centre for Advanced 2D Materials
National University of Singapore
6 Science Drive 2, Singapore 117543, Singapore

T. J. Duffin, Dr. K. S. Kumar, Prof. C. A. Nijhuis
Department of Chemistry
National University of Singapore
3 Science Drive 3, Singapore 117543, Singapore

T. J. Duffin, Dr. K. S. Kumar, Prof. C. A. Nijhuis
NUSNNI-Nanocore
National University of Singapore
Singapore 117411, Singapore

T. J. Duffin, Dr. K. S. Kumar, Prof. C. A. Nijhuis
Centre for Advanced 2D Materials and Graphene Research Centre
National University of Singapore
6 Science Drive 2, Singapore 1175464, Singapore

T. J. Duffin, Dr. K. S. Kumar, Prof. C. A. Nijhuis
National University of Singapore Graduate School for Integrative Sciences and Engineering
National University of Singapore
28 Medical Drive, Singapore 117456, Singapore

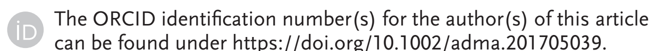
The ORCID identification number(s) for the author(s) of this article can be found under https://doi.org/10.1002/adma.201705039.

DOI: 10.1002/adma.201705039

 © 2017 WILEY-VCH Verlag GmbH & Co. KGaA, Weinheim

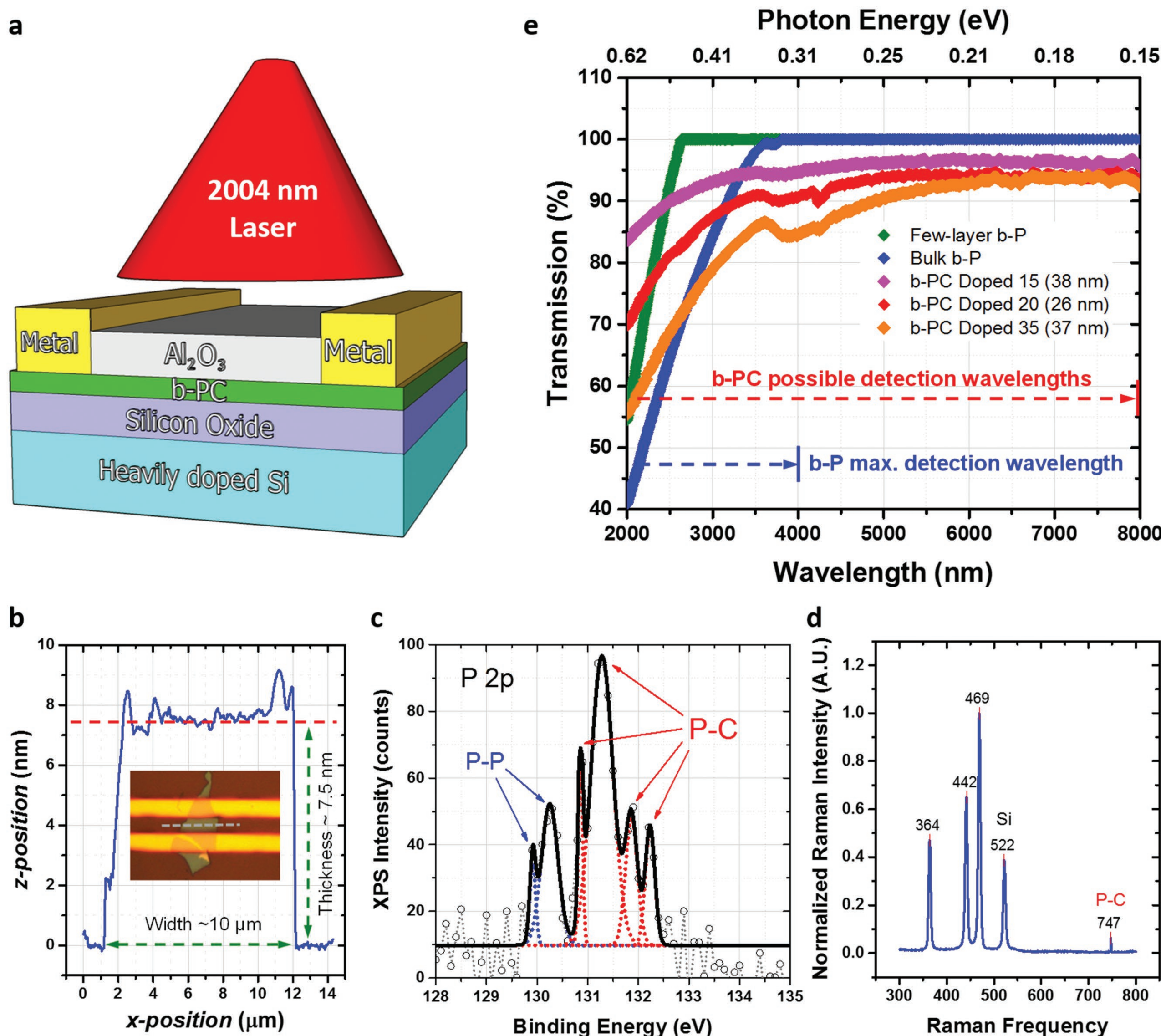

Figure 1. The physical structure and material characteristics of b-PC phototransistor. a) Schematic diagram of the b-PC phototransistor. The metal contact is made of sputtered Au/Ni (30 nm/1 nm). b) The AFM of the b-PC phototransistor. The average thickness across the channel width of ≈10 µm is ≈7.5 nm. The micrograph shown in the inset is the magnified image of the b-PC phototransistor. The two yellow horizontal bars are the Au/Ni contact of the transistor. c) The XPS spectra of the P 2p core level in b-PC. The binding energy at 130.9, 131.3, 131.9, 132.2, and 132.1 eV can all be assigned to the P—C bonds. The b-PC also exhibits the spin-orbit split doublet of an exfoliated b-P at ≈129.9 and 130.2 eV, consistent with previous XPS measurements on a b-P bulk crystals.[15] d) The Raman spectra of the b-PC. The sample possesses a prominent b-PC phonon mode at 747 cm^{-1} in addition to the three phonon modes of b-P at 364, 442, and 469 cm^{-1}. The P—C bond stretching modes (670–780 cm^{-1}), are based on theoretical calculations reported in the literature.[20] e) The absorption spectra of a b-P and b-PC taken using Fourier transform infrared spectroscopy (FTIR). Doped 15 referred to a doping cycle of 15 and vice versa for Doped 20 and Doped 35 (see the Experimental Section).

intrinsic absorption spectrum ranging from the visible to the FIR spectrum. Here, we report a high-performance black phosphorus carbide (b-PC) phototransistor fabricated via a novel carbon doping technique,[15] which achieved a peak responsivity of ≈2163 A W^{-1} and a shot noise equivalent power (NEP_{shot}) of 1.3 fW $Hz^{-1/2}$ at 2004 nm. In addition, we show that a minimum response time of ≈0.7 ns is tunable by gating effect for high-speed application, along with an extended spectrum with nonzero absorption up to 8000 nm. Under the same excitation power (≈13 nW), the responsivity and detectivity of the b-PC phototransistor in ambient and room temperature conditions are currently ahead of recently reported photodetectors based on 2DMs operating with a bias voltage of 0.2 V.

Figure 1a shows the schematic diagram of the b-PC phototransistor. Few-layer b-P is first mechanically exfoliated from a bulk single-crystal b-P (purity 99.998%, Smart Element) onto a degenerately doped Si substrate with a pregrown thermal oxide (300 nm) at the surface. Immediately after the exfoliation, the sample is doped with hydrocarbons inside an atomic layer deposition (Savannah ALD) chamber at 0.3 Torr using only trimethylaluminum (TMA) precursor pulsing at a low substrate temperature of 120 °C for 15 ms and purged

© 2017 WILEY-VCH Verlag GmbH & Co. KGaA, Weinheim

with N_2 at 20 sccm for 10 s. The pulsing and purging of TMA and N_2 is then repeated for 20 cycles. The contact patterns on the channel are written using a Laser Writer (LW405B) and the Au/Ni (30 nm/1 nm) metals are deposited by sputtering (AJA ATC-2200 UHV Sputter). The sample is then bathe in acetone for 15 min during which, any unwanted metals will be lifted off from the sample, leaving only the patterned metal contacts on the channel. Lastly, the contact and the channel are thermally treated to 200 °C for ≈53 min in an atomic layer deposition chamber while at the same time, an Al_2O_3 passivation layer (20 nm) is grown on the device with TMA (pulsed at 15 ms) and water (pulsed at 15 ms) as the precursors, and purged with N_2 at 20 sccm for 8 s (see the Supporting Information for process flow). An optical micrograph of the fabricated b-PC phototransistor is as shown in the inset of Figure 1b, where a sample (shown as a dashed gray line in the inset) of the physical profile of the channel is taken using an atomic force microscopy (AFM). From the AFM, we can see that the average thickness of the 5 µm long b-PC phototransistor is ≈7.5 nm and the width of the channel is ≈10 µm. Its hole field-effect mobility (μ_{FE}) is calculated to be 382 $cm^2 V^{-1} s^{-1}$ at a drain-to-source bias voltage (V_D) of –0.2 V (see the Supporting Information for computation details). The X-ray photoelectron spectroscopy (XPS) spectra of the P 2p core level of this b-PC sample are shown in Figure 1c. The binding energy at 130.9, 131.3, 131.9, 132.2, and 132.1 eV can all be assigned to the P—C bonds based on references related to either carbon doped b-P,[15] or phosphorus-doped carbon materials.[16] Figure 1d shows the Raman spectra of the b-PC. The sample possesses a phonon mode of b-PC at 747 cm^{-1} in addition to the three phonon modes at 365, 444, and 469 cm^{-1} typically measured in b-P.[17–19] The P—C bond stretching modes (670–780 cm^{-1}) are based on the theoretical calculations reported in the literature,[20] whereas the G band of hybridized sp^2 C—C bonding is typically found in between 1500 and 1600 cm^{-1}. Besides the Raman spectra, we have also measured the absorption spectrum of our b-PC sample. The absorption spectra taken using a Fourier transform infrared spectroscopy are shown in Figure 1e. It displays the absorbance (expressed in terms of transmission) measured as a function of wavelengths for b-PC with different thicknesses and doping cycles. This absorption spectrum agrees well with the bandgap energy (≈0.12 eV)[15] calculated from the first principles for a monolayer and composite b-PC.[21]

The optical measurement was performed on a probe station in ambient condition using a laser diode guided through an optical fiber with a numerical aperture of 0.11 and a mode field diameter of 13 µm. The laser is placed vertically ≈3 mm away from the sample via a microprobe and the calculated spot size of the laser at this height is 673 µm (see the Supporting Information for more details). The output and transfer characteristics of the b-PC phototransistor are first measured without any illumination and then under illumination at different excitation power. **Figure 2**a,b shows the dark current ($I_{D,dark}$) at different operating voltages (V_G) and the changes in output drain current ($I_{D,illuminated}$) of the b-PC phototransistor when it is being excited by a laser with a wavelength of 2004 nm at $V_G = -40$ V (see the Supporting Information for $I_{D,illuminated}$ at $V_G = 0$ and +40 V). The photocurrent at different incident excitation power density (P_{in}) and V_G are then extracted from the output characteristic of the phototransistor, $I_{ph} = |I_{D,illuminated}| - |I_{D,dark}|$, and plotted in Figure 2c,d, where the incident power on the active region (P_{device}) is defined as $P_{device} = P_{in} \times L \times W$, and both L and W are, respectively, the channel length and width of the phototransistor. The observed photoconductive effect of our photodetector with V_G can be explained by a simple energy-band diagram as shown in Figure 2e. When there is no illumination, V_G and V_D, the device is in its equilibrium state, characterized by small Schottky barriers (Φ_B) at the contacts. Illuminating the device in its OFF state ($V_G > V_T$), where V_T is the threshold voltage of the phototransistor, results in light absorption and excitation of electron–hole pairs, which can be extracted by applying a V_D. This OFF-state photocurrent would then increase with an increase in either P_{in} or V_D, as any increase in excitation power will result in more excitation of electron–hole pairs whilst an increase in V_D will lead to a reduction of the carrier transit time, $\tau_{transit} = \frac{L^2}{\mu_{FE} V_D}$, where μ_{FE} is the transistor's hole field effect mobility, and L is the channel length. In contrast to P_{device} or V_D, any increase in V_G (i.e., more positive) increases the Schottky barriers at the contacts, resulting in a less efficient OFF-state photocurrent extraction. Similarly, the ON-state ($V_G < V_T$) photocurrent would also increase with either an increase in P_{device} or V_D, or a decrease in V_G.

Next, we study the photoresponse of the b-PC photodetector at different P_{device} for the same excitation wavelength of 2004 nm. **Figure 3**a,b shows the responsivity (R), where $R = \frac{I_{ph}}{P_{device}}$, of the b-PC phototransistor to this excitation wavelength at different P_{device}, V_G, and V_D. Unlike the photocurrent, the responsivity would increase with decreasing P_{device} at all V_G as the photocarrier lifetime of the majority carrier (i.e., hole) is longer in a photoconductor under a lower excitation power.[22] This would allow the charge carrier to flow multiple times from the source to the drain before it recombines with a minority carrier (i.e., electron). In other words, when less electron–hole pairs (i.e., at low excitation power) are being created in the channel to fill up the trap centers, relatively more minority carrier traps would be available and thus the photocarrier lifetime of the majority carriers would be extended. This is because fewer minority carriers are available for recombination since they are being captured by the traps. On the other hand, just like the photocurrent, the responsivity would increase with V_D at all V_G due to a reduction of the carrier transit time when the biased voltage is increased. At room temperature, a high responsivity (R) of ≈2163 A W^{-1} for an excitation wavelength of 2004 nm can be achieved with a low V_D of –0.2 V and P_{device} of ≈281 pW (i.e., the lowest limit of our lasing power, at ≈0.6 mW cm^{-2}). This responsivity is not only higher than commercial solid-state detectors like silicon photodiodes in the visible spectrum (≈0.5 A W^{-1}),[23] and InGaAs detectors in the MIR spectrum (≈1.2 A W^{-1}),[24] but also 2D broadband detectors like the graphene photodetector (10 mA W^{-1}),[12] and b-AsP photodetector (180 mA W^{-1} at an excitation power of 70 nW and wavelength of 3662 nm).[11] Although a hybrid graphene detector with PbS quantum dots has demonstrated so far the largest responsivity in the visible range (5×10^7 A W^{-1} at an excitation power of 10 fW and wavelength of 600 nm),[2] the photocarriers lifetime via photogating effect has slowed its response time to 0.1 s and narrowed its detection window to 1600 nm due to the quantum

© 2017 WILEY-VCH Verlag GmbH & Co. KGaA, Weinheim

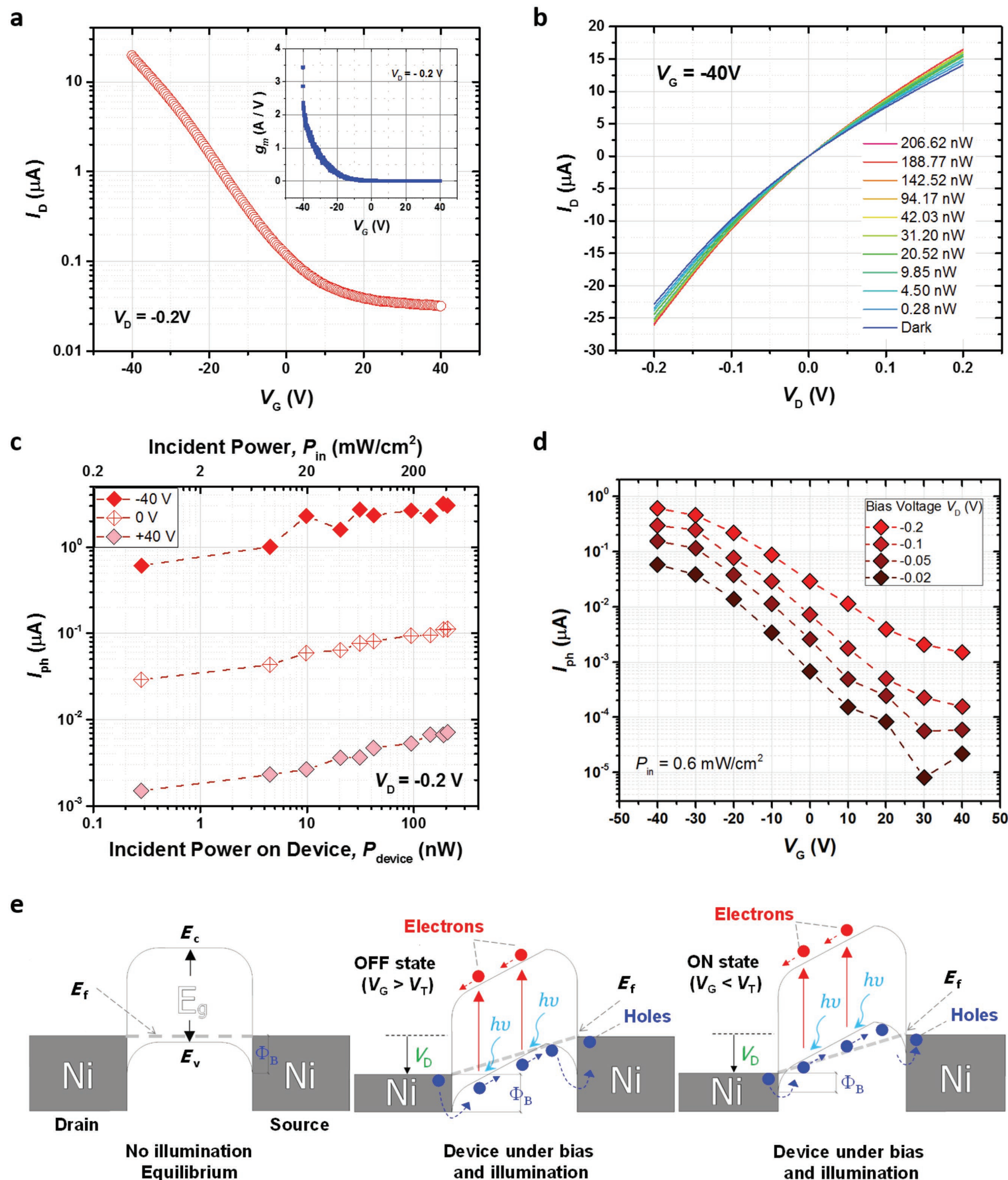

Figure 2. Electrical performance of the b-PC phototransistor at room temperature. a) The transfers characteristic and transconductance, g_m (inset), of the b-PC phototransistor at a drain voltage of −0.2 V. b) The drain current (I_D) of b-PC phototransistor at V_G = −40 V with different P_{device} from a laser with an excitation wavelength of 2004 nm. c,d) The photocurrent (I_{ph}) generated in the b-PC phototransistor from an excitation wavelength of 2004 nm at different V_D, V_G, and P_{device}. e) The energy-band diagram illustrating the operation of b-PC phototransistor at different V_G (ON and OFF state) with and without illumination.

© 2017 WILEY-VCH Verlag GmbH & Co. KGaA, Weinheim

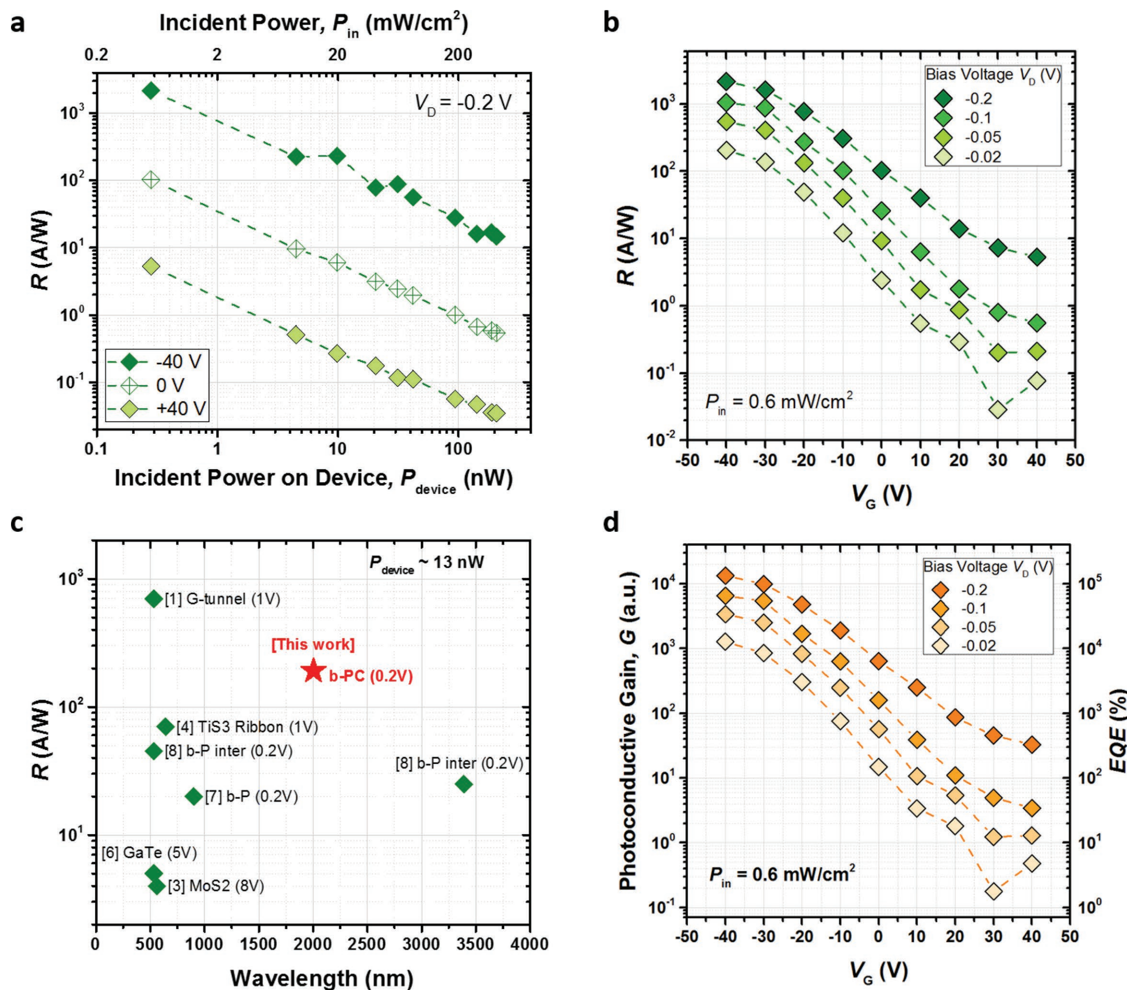

Figure 3. The responsivity (R), external quantum efficiency (EQE), and photoconductive gain (G) of b-PC phototransistor at ambient room temperature. a,b) The R of the b-PC photodetector at an excitation wavelength of 2004 nm with different V_D, V_G, and P_{device}. c) The responsivity of b-PC as compared to recently reported 2DMs photodetectors measured at the same amount of incident power on the active region ($P_{device} \approx 13$ nW). The x-axis represents the excitation wavelength of the laser and the voltage in bracket is the amount of bias voltage or drain voltage applied on the device. d) The G and EQE of the b-PC photodetector at an excitation wavelength of 2004 nm with different V_D and V_G. All dashed lines in the figures are drawn as an eye guide to show the variations of the parameters.

dots structure. Since responsivity depends directly on P_{device} and V_D, Figure 3c shows the responsivity of b-PC phototransistor and all recently reported photodetectors at the same excitation power of $P_{device} \approx 13$ nW. We can see the b-PC phototransistor as having the highest responsivity among all recently reported photodetectors that operate with a bias voltage of 0.2 V. Other than responsivity, we have also shown in Figure 3d the external quantum efficiency, $\mathrm{EQE} = \frac{n_e}{n_{ph}}$, of the b-PC phototransistor, where n_e is the number of the charge carriers in the photocurrent and n_{ph} is the number of impinging excitation photons on the active region. The photoconductive gain is defined as $= \frac{n_e}{n_{ab}}$, where n_{ab} is the number of photons being absorbed (absorption ≈10%; see the Supporting Information for details). At $V_G = -40$ V and $V_D = -0.2$ V, Figure 3d shows the EQE and G peak at $\approx 1.3 \times 10^5$% and 1.3×10^4, respectively. When the b-PC phototransistor is set to operate in the OFF state where there is little or no transconductance gain, the magnitude of this photodetection gain can be quantified based on a simple physical picture incorporating the typical lifetimes for electrons and holes carriers. Photoexcited holes carriers in the b-PC channel are first separated from the photoexcited electrons and drift to the drain by the applied V_D, with a typical timescale of $\tau_{transit} = \frac{L^2}{\mu_{FE} V_D}$. Some of the photoexcited electrons would inevitably be held up by the minority carrier traps at the surface with a timescale of $\tau_{lifetime}$ (see the Supporting Information for details). Charge conservation in the channel would lead to hole replenishment from the source as soon as a hole carrier reaches the drain. As a result, the same photogenerated hole carrier from a single electron–hole pair excited by a photon would get to circulate multiple times in the b-PC channel, leading to photoconductive gain where $G = \frac{\tau_{lifetime}}{\tau_{transit}}$, indicating the importance of long lifetime and high carrier mobility.

Since a photoconductive detector may exhibit a high dark current and its photocurrent is also related to its active

© 2017 WILEY-VCH Verlag GmbH & Co. KGaA, Weinheim

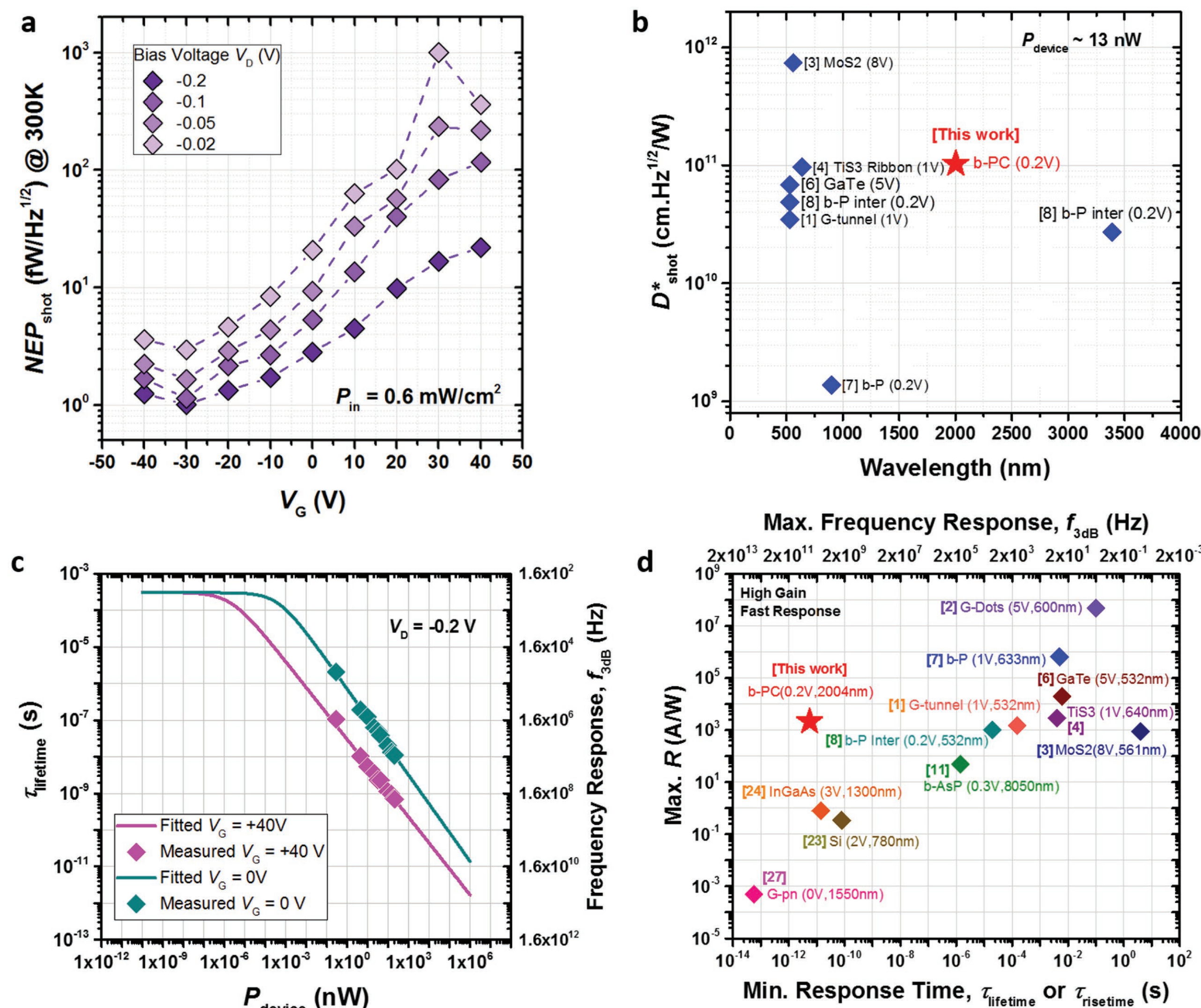

Figure 4. The photoconductive performance of b-PC phototransistor at ambient room temperature and recently reported photodetectors. a,b) The NEP_{shot} and the detectivity (D^*) of b-PC phototransistor against the operating gate voltage and other recently reported photodetectors based on 2DMs measured at the same amount of incident power ($P_{device} \approx 13$ nW). The *x*-axis in (b) represents the excitation wavelength of the laser and the voltage in bracket is the amount of bias voltage applied on the device. c) The measured carrier lifetime and 3-dB cutoff frequency response of the b-PC phototransistor under different P_{device} and the fitted values from Hornbeck–Haynes model. d) The peak responsivity and minimum response time of b-PC phototransistor are achieved at $V_G = -40$ V and +40 V, respectively, as compared to other recently reported top performing photodetectors based on 2DMs. The values in bracket represent the applied bias voltage and the excitation wavelength. The respective reference values are obtained from the followings: G-tunnel (rise time from graphene with tunnel barrier),[1] b-P Inter (carrier lifetime from black phosphorus with interdigitated electrodes),[8] b-P (rise time from black phosphorus),[7] TiS_3 ribbon (rise time from TiS_3 nanoribbon),[4] MoS_2 (rise time from monolayer MoS_2),[3] GaTe (rise time from multilayer GaTe),[6] G-Dots (carrier lifetime from graphene with PbS quantum dots),[2] b-AsP (carrier lifetime from black arsenic phosphorus),[11] G-pn (carrier lifetime from graphene),[27] InGaAs (rise time from commercial InGaAs PIN),[24] and Si (rise time from commercial Si PIN).[23]

detection area, a more complete assessment of the detector performance must include its noise equivalent power (NEP) and specific detectivity (D^*). The NEP is defined as the lowest optical power that yields a unity signal-to-noise ratio for a normalized bandwidth of 1 Hz and can be calculated by dividing the noise current spectral density (PSD) of the detector at a modulation frequency of 1 Hz by its maximum responsivity, i.e., $\mathrm{NEP} = \frac{\mathrm{PSD}_{1\mathrm{Hz}}}{R_{\max}}$. The PSD can be obtained by measuring the dark current of the detector via a fast Fourier transform spectrum analyzer and the results reflect the overall noise effect due to thermal noise, flicker noise ($1/f$),[25] and shot noise of the detector. For a photoconductive detector limited only by its shot noise, the equivalent noise current density of the shot noise ($\mathrm{PSD}_{\mathrm{shot}}$) can be normalized from the root mean square of its dark current fluctuations as, $\mathrm{PSD}_{\mathrm{shot}} = \frac{\sqrt{2\,q\,I_D\Delta f}}{\Delta f}$, where $\Delta f =$ 1 Hz, I_D is the drain current in the dark at maximum responsivity, and q is the electron charge. With this expression, we can calculate the shot noise equivalent power, $\mathrm{NEP}_{\mathrm{shot}} = \frac{\mathrm{PSD}_{\mathrm{shot}}}{R_{\max}}$, for the b-PC phototransistor at different V_G (**Figure 4**a). At $V_D =$ -0.2 V and $V_G = -40$ V, the $\mathrm{NEP}_{\mathrm{shot}} \approx 1.3 \times 10^{-15}$ W Hz$^{-1/2}$,

© 2017 WILEY-VCH Verlag GmbH & Co. KGaA, Weinheim

indicating that infrared radiation in the femto-watt range can be detected above the shot noise level of this b-PC phototransistor with an integration time of 0.5 s. Since the spectral density of thermal and shot noise are not frequency dependent,[25] and thermal noise is lower than the shot noise at all V_D and V_G (see the Supporting Information for details), NEP_{shot} is a good white noise performance representation for our b-PC phototransistor. This performance is better than the b-P detector with an optimized photocarrier collector ($NEP_{shot} \approx 4.6 \times 10^{-14}$ W $Hz^{-1/2}$ with a dark current of 50 μA at $V_D = 0.5$ V and $V_G = 5$ V),[8] and the graphene detector with a tunnel barrier that enhances its photogating effect ($NEP_{shot} \approx 4.3 \times 10^{-15}$ W $Hz^{-1/2}$ with an operating dark current of 190 μA at $V_D = 1$ V and $V_G = -40$ V).[1] To compare detectors with different geometries, we can compute its specific detectivity, $D^*_{shot} = \frac{\sqrt{\text{Active area}}}{NEP_{shot}}$. With the same amount of excitation power, $P_{device} \approx 13$ nW, Figure 4b shows b-PC phototransistor as having the highest detectivity among all recently reported photodetectors that operate with a bias voltage of 0.2 V.

Lastly, we analyze the fundamental operating speed of this b-PC phototransistor. This can be determined from the average lifetime of the photocarriers in the channel. Using the transit time ($\tau_{transit} \approx 3.27$ ns) calculated from our hole carrier mobility (≈382 cm^2 V^{-1} s^{-1}), we can obtain the carrier lifetime of our b-PC phototransistor from the photoconductive gain. Figure 4c shows the measured carrier lifetime and 3-dB cutoff frequency of the b-PC phototransistor under different V_G and P_{device} along with the respective fitted values from the Hornbeck–Haynes model.[26] From the figures, we can see the b-PC phototransistor is having a calculated response time of ≈0.7 ns (or ≈0.2 GHz) at $V_G = +40$ V with $V_D = -0.2$ V and $P_{device} \approx 207$ nW. By using the model, we can extrapolate the carrier lifetime and 3-dB cutoff frequency of the b-PC phototransistor to an excitation power, P_{device}, not available to us in our setup (see the Supporting Information for details). According to the model, the fundamental response time can reach up to ≈14 ps (or ≈11 GHz) at $P_{device} \approx 1$ mW with $V_G = +40$ V and $V_D = -0.2$ V. The carrier lifetime at low excitation power (τ_0), which does not vary with P_{device}, is ≈0.3 ms (or ≈510 Hz). Figure 4d shows the maximum responsivity and minimum response time of our b-PC phototransistor and other 2DMs photodetectors regardless of their bias voltage, excitation wavelength, and power. As is evident in Figure 4d, even though the b-PC phototransistor does not have the highest responsivity or the shortest response time, it is at the location nearest to the most desired region for a photodetector, where responsivity is high and response is fast. In fact, according to the Hornbeck–Haynes model, the gain bandwidth product (GBW) of any phototransistor will depend only on the transit time (i.e., μ_{FE}) of the phototransistor, $GBW = \frac{1}{2\pi\tau_{transit}}$ (see the Supporting Information for details on Hornbeck–Haynes model).[26] This means that for the same responsivity, the b-PC phototransistor will always enjoy a speed advantage over other 2DMs as it currently has the highest theoretical carrier mobility, approximately five times larger than the maximum value in b-P, and among all known 2DMs except graphene.[15,21] Having said that, we also like to point out that carrier mobility is not an end to itself. As we all know, while graphene photodetector may have the shortest response time of ≈0.6 fs at $P_{device} \approx 3$ mW[27] among all known 2DMs, its responsivity cannot be tuned to a level higher than the b-PC phototransistor due to ultrafast hot carrier recombination time, the small photoactive region, and weak optical absorption.[1] Although inserting a tunnel barrier into graphene[1] or hybridizing graphene with quantum dots[2] can greatly improve graphene's responsivity by extending the photocarrier lifetime via traps engineering, the enhancement come with a price on its absorption spectrum which is shortened to 1600 nm,[2] and its response time which is lengthened from 0.6 fs to a range of 0.1 ms to 1 s[1,2] apart from its fabrication complexity.

In summary, we have demonstrated a novel b-PC phototransistor with a wide absorption spectrum up to 8000 nm and a tunable responsivity and response time at an excitation wavelength of 2004 nm. The b-PC phototransistor can be tuned to operate with a peak responsivity of ≈2163 A W^{-1} for low light condition or with a minimum response time of ≈0.7 ns for high-speed applications. Its $NEP_{shot} \approx 1.3$ fW $Hz^{-1/2}$ indicates that infrared radiation in the femto-watt range can be detected above the shot noise level of this phototransistor. Under the same excitation power, its performance in responsivity and detectivity in ambient and room temperature conditions are currently ahead of all recent top-performing 2DMs photodetectors that operate with a bias voltage of 0.2 V. It also has the best combination of maximum responsivity and minimum response time among all top-performing photodetectors based on 2DMs regardless of their bias voltage, excitation wavelength, and power. We believe that the wide intrinsic absorption spectrum and operating versatility demonstrated in our b-PC phototransistor would make b-PC a very attractive material for use as a sensor in flexible optoelectronics in the coming age of the IoT.

Supporting Information

Supporting Information is available from the Wiley Online Library or from the author.

Acknowledgements

This research was supported by the National University of Singapore Faculty Research Committee Grants (R-263-000-B21-133 and R-263-000-B21-731), A*STAR Science and Engineering Research Council Grant (No. 152-70-00013), National Research Foundation Competitive Research Programs (NRF-CRP15-2015-01, NRF-CRP15-2015-02, and NRF-CRP17-2017-08), and by the National Research Foundation, Prime Minister's Office, Singapore under its MediumSized Centre program.

Conflict of Interest

The authors declare no conflict of interest.

© 2017 WILEY-VCH Verlag GmbH & Co. KGaA, Weinheim

Keywords

black phosphorus carbide, broadband detectors, infrared detectors, low noise, tunable responsivity

Received: September 4, 2017
Revised: October 4, 2017
Published online:

[1] C.-H. Liu, Y.-C. Chang, T. B. Norris, Z. Zhong, *Nat. Nanotechnol.* **2014**, *9*, 273.
[2] G. Konstantatos, M. Badioli, L. Gaudreau, J. Osmond, M. Bernechea, F. P. G. de Arquer, F. Gatti, F. H. L. Koppens, *Nat. Nanotechnol.* **2012**, *7*, 363.
[3] O. Lopez-Sanchez, D. Lembke, M. Kayci, A. Radenovic, A. Kis, *Nat. Nanotechnol.* **2013**, *8*, 497.
[4] J. O. Island, M. Buscema, M. Barawi, J. M. Clamagirand, J. R. Ares, C. Sánchez, I. J. Ferrer, G. A. Steele, H. S. J. van der Zant, A. Castellanos-Gomez, *Adv. Opt. Mater.* **2014**, *2*, 641.
[5] a) Z. P. Ling, R. Yang, J. W. Chai, S. J. Wang, W. S. Leong, Y. Tong, D. Lei, Q. Zhou, X. Gong, D. Z. Chi, K.-W. Ang, *Opt. Express* **2015**, *23*, 13580; b) Z.-P. Ling, R. Yang, J.-W. Chai, S.-J. Wang, Y. Tong, Q. Zhou, X. Gong, D.-Z. Chi, K.-W. Ang, in *2015 IEEE International Wireless Symposium*, IEEE, Piscataway, NJ, USA **2015**, https://doi.org/10.1109/IEEE-IWS.2015.7164640.
[6] F. Liu, H. Shimotani, H. Shang, T. Kanagasekaran, V. Zólyomi, N. Drummond, V. I. Fal'ko, K. Tanigaki, *ACS Nano* **2014**, *8*, 752.
[7] M. Huang, M. Wang, C. Chen, Z. Ma, X. Li, J. Han, Y. Wu, *Adv. Mater.* **2016**, *28*, 3481.
[8] Q. Guo, A. Pospischil, M. Bhuiyan, H. Jiang, H. Tian, D. Farmer, B. Deng, C. Li, S. J. Han, H. Wang, Q. Xia, T. P. Ma, T. Mueller, F. Xia, *Nano Lett.* **2016**, *16*, 4648.
[9] Y. Liu, Y. Cai, G. Zhang, Y.-W. Zhang, K.-W. Ang, *Adv. Funct. Mater.* **2017**, *27*, 1604638.
[10] L. Huang, W. C. Tan, L. Wang, B. Dong, C. Lee, K.-W. Ang, *ACS Appl. Mater. Interfaces* **2017**, *9*, 36130.
[11] M. Long, A. Gao, P. Wang, H. Xia, C. Ott, C. Pan, Y. Fu, E. Liu, X. Chen, W. Lu, T. Nilges, J. Xu, X. Wang, W. Hu, F. Miao, *Sci. Adv.* **2017**, *3*, e1700589.
[12] M. Buscema, J. O. Island, D. J. Groenendijk, S. I. Blanter, G. A. Steele, H. S. van der Zant, A. Castellanos-Gomez, *Chem. Soc. Rev.* **2015**, *44*, 3691.
[13] S. C. Dhanabalan, J. S. Ponraj, H. Zhang, Q. Bao, *Nanoscale* **2016**, *8*, 6410.
[14] Y. Zhang, T.-T. Tang, C. Girit, Z. Hao, M. C. Martin, A. Zettl, M. F. Crommie, Y. R. Shen, F. Wang, *Nature* **2009**, *459*, 820.
[15] W. C. Tan, Y. Cai, R. J. Ng, L. Huang, X. Feng, G. Zhang, Y.-W. Zhang, C. A. Nijhuis, X. Liu, K.-W. Ang, *Adv. Mater.* **2017**, *29*, 1700503.
[16] a) Y. Wen, B. Wang, C. Huang, L. Wang, D. Hulicova-Jurcakova, *Chem. Eur. J.* **2015**, *21*, 80; b) R. Li, Z. Wei, X. Gou, W. Xu, *RSC Adv.* **2013**, *3*, 9978.
[17] a) Z.-P. Ling, S. Sarkar, S. Mathew, J.-T. Zhu, K. Gopinadhan, T. Venkatesan, K.-W. Ang, *Sci. Rep.* **2015**, *5*, 18000; b) Z.-P. Ling, K. Majumdar, S. Sarkar, S. Mathew, J.-T. Zhu, K. Gopinadhan, T. Venkatesan, K.-W. Ang, in *2016 Int. Symp. on VLSI Technology, Systems and Application*, IEEE, Piscataway, NJ, USA **2016**, https://doi.org/10.1109/VLSI-TSA.2016.7480535.
[18] a) Z.-P. Ling, J.-T. Zhu, X. Liu, K.-W. Ang, *Sci. Rep.* **2016**, *6*, 26609; b) Z.-P. Ling, X. Feng, H. Jiang, Z. He, X. Liu, K.-W. Ang, in *2016 IEEE Silicon Nanoelectronics Workshop*, IEEE, Piscataway, NJ, USA **2016**, pp. 24–25, https://doi.org/10.1109/SNW.2016.7577967.
[19] a) Y. Liu, K.-W. Ang, *ACS Nano* **2017**, *11*, 7416; b) X. Liu, K.-W. Ang, W. Yu, J. He, X. Feng, Q. Liu, H. Jiang, D. Tang, J. Wen, Y. Lu, W. Liu, P. Cao, S. Han, Js. Wu, W. Liu, X. Wang, D. Zhu, Z. He, *Sci. Rep.* **2016**, *6*, 24920.
[20] a) J. Sun, G. Zheng, H.-W. Lee, N. Liu, H. Wang, H. Yao, W. Yang, Y. Cui, *Nano Lett.* **2014**, *14*, 4573; b) F. Claeyssens, G. M. Fuge, N. L. Allan, P. W. May, M. N. R. Ashfold, *Dalton Trans.* **2004**, *0*, 3085.
[21] a) G. Wang, R. Pandey, S. P. Karna, *Nanoscale* **2016**, *8*, 8819; b) J. Guan, D. Liu, Z. Zhu, D. Tománek, *Nano Lett.* **2016**, *16*, 3247.
[22] J. A. Hornbeck, J. R. Haynes, *Phys. Rev.* **1955**, *97*, 311.
[23] K. K. Hamamatsu, "Si Photodiodes," (Ed: Hamamatsu-Photonics), **2017**.
[24] K. K. Hamamatsu, "InGaAs Photodiodes," (Ed: Hamamatsu-Photonics) **2015**.
[25] A. A. Balandin, *Nat. Nanotechnol.* **2013**, *8*, 549.
[26] C. Soci, A. Zhang, B. Xiang, S. A. Dayeh, D. P. R. Aplin, J. Park, X. Y. Bao, Y. H. Lo, D. Wang, *Nano Lett.* **2007**, *7*, 1003.
[27] F. Xia, T. Mueller, Y.-M. Lin, A. Valdes-Garcia, P. Avouris, *Nat. Nanotechnol.* **2009**, *4*, 839.

© 2017 WILEY-VCH Verlag GmbH & Co. KGaA, Weinheim